2011 American Control Conference
on O'Farrell Street, San Francisco, CA, USA
June 29 - July 01, 2011

Trajectory Determination for Energy Efficient Autonomous Soaring

Wilson B. Kagabo and Jason R. Kolodziej

Abstract—**Unmanned Aerial Gliders (UAG) use atmospheric energy in its different forms to remain aloft for extended flight durations. This UAG's aim is to extract atmospheric thermal energy and use it to supplement its battery energy usage and increase the mission period. Given an identified atmospheric thermal of known strength and location; current wind speed and direction; battery level; altitude and location of the UAG; and estimating the expected altitude gain from the thermal, is it possible to make an energy-efficient based motivation to fly to an atmospheric thermal so as to achieve UAG extended flight time? For this work it is assumed that candidate atmospheric thermal locations are of known longitude/latitude location, size, and strength. An algorithm, based on a fuzzy logic approach, is then developed to incorporate all available information with the current UAG status to provide an energy-based recommendation to modify the flight path from the nominal mission trajectory. Research, development, and simulation of the decision-making algorithm is the primary focus of this work. Three models are developed: Battery Usage Model (BUM), Altitude Gain Model (AGM), and Intelligent Decision Model (IDM).**

I. Introduction

Identifying atmospheric thermals before deciding to use them for gliding is an area of active research. The strategies in place so far cannot predict with certainty the presence of an atmospheric thermal at a given location. Some research has been conducted explaining analytical ways to fly in or through atmospheric thermals when their locations are known. What has not been researched is how one can identify an atmospheric thermal ahead of time and analyze it against other mission parameters and variables so as to make an informed decision of whether to or not to fly to it.

Over the years, studies in UAV autonomous soaring have led to resourceful literature on how to extract atmospheric energy from dynamic air and use it to extend flight time specifically the work by Allen [1], [2], [3], Langelaan [4], Langelaan, et.al. [5], and Edwards [6]. NASA Dryden Flight Research Center with Allen pioneered the concept of autonomous soaring by designing and implementing an algorithm that searches atmospheric thermals and utilizes them for autonomous soaring of glider-based Unmanned Aerial Systems. Edwards' work at North Caroline State University and the Naval Research Laboratory is a continuation of this research. His research minimized development time and cost of Allen's algorithm through the development of an off-board implementation using an approach based on the neural network method initially presented by Wharington [7] and built a new hybrid algorithm. The atmospheric thermal identification model presented by Edwards is used to confirm that in fact a UAV glider is in an atmospheric thermal.

While this research is critical when flying within the thermal, however, research is needed to bridge the gap between time of atmospheric thermal identification and soaring. The UAG autopilot need to know atmospheric thermal locations and the energy savings expected from each thermal before deciding to whether soar it or not. This work builds on the assumption that the strength, size, latitude and longitude location of an atmospheric thermal are identified from an external source, specifically a remote sensing via infrared thermal image. The optimal trajectory is then planned using a Dubins Set optimal path planning approach. The atmospheric thermal is analyzed against other parameters of the UAG such as current fuel (battery level or otherwise), current location, and UAG dynamic properties so as to determine the fuel cost and expected altitude gain from the thermal. The thermal path is then compared with a nominal path and the more energy–efficient path of the two is considered based on the time criticality of the mission.

Ying and Zhao's research [8] in 2005 discusses optimal energy-efficient flight trajectories of a generic UAV flying through a vertical moving atmospheric thermal. Their work compares the fuel efficiency of these optimal trajectories with those of reference optimal flights in the absence of atmospheric thermal and the results suggest significant improvements in the UAV fuel consumption when atmospheric thermal trajectories are undertaken.

For this work, the UAG is required to fly to different waypoints. Its mission objective(s) include but not limited to: inspecting suspicious locations (intelligence and reconnaissance), patrolling international borders and wildfire remote sensing. Most existing research in autonomous soaring shows fairly random flight paths but this work attempts to incorporate the atmospheric energy available into the mission objectives.

II. Model Development

A. Battery Usage Model

L.E. Dubins pioneering work of 1957 [9] on trajectory generation theory is the most fundamental benchmark theory many researchers over the years have successfully relied on to determine the optimal two-dimensional trajectory for moving vehicles both ground and air based. In his work a method to determine a series of circular arcs of known radius of curvature and straight line segment is developed,

Manuscript received September 22, 2010.

W. B. Kagabo was a Graduate Student with Rochester Institute of Technology, Rochester, NY 14623 USA. He is now with the Kigali Institute of Science and Technology P.O Box 3900 Kigali, Rwanda (e-mail: kbvilson@yahoo.com).

J. R. Kolodziej is an Assistant Professor with the Mechanical Engineering Department, Rochester Institute of Technology, Rochester, NY 14623 USA. (phone: 585-475-4313; fax: 585-475-7710; e-mail: jrkeme@rit.edu).

which when connected together, determines the shortest trajectory between two points provided the turning radius, initial and final heading angles are specified. The Dubins work proves that any shortest trajectory comprises of only three segments, which can be arranged in the order of CCC (Curved-Curved-Curved) or CSC (Curved-Straight-Curved). Where C is an arc of radius R_{arc} and can be either a turn right "R" or a turn left "L" and "S" is the straight line. Using elementary transformations shown in (1) through (3) and the above criteria, Shkel and Lumelsky [10] were able to confirm that there are only six admissible Dubins Set trajectories $\{RLR, LRL, RSR, LSL, RSL, LSR\}$. This path planning technique has recently been successful in trajectory-planning problems for unmanned aerial vehicles [11]

$$L_v(x, y, \phi) = (x + R_{arc}sin(\phi + v) - R_{arc}sin\phi, y - R_{arc}cos(\phi + v) + R_{arc}v) \quad (1)$$

$$R_v(x, y, \phi) = (x - R_{arc}sin(\phi - v) + R_{arc}sin\phi, y + R_{arc}cos(\phi - v) - R_{arc}\cos\phi, \phi - v) \quad (2)$$

$$S_v(x, y, \phi) = (x + vcos\phi, y + vsin\phi, \phi) \quad (3)$$

where; L_v, R_v and S_v are the motion operators corresponding to the left-turn, right-turn and straight-line respectively; x, y, ϕ and R_{arc} are the four inputs to the Dubins trajectory and they represent longitude, latitude, heading angle and turning radius of the aircraft, and v is the segment length. The radius of the arc depends on the turning radius of the aircraft. Longitude/latitude values read from the Global Positioning System (GPS) or maps are converted from degrees into Cartesian coordinates for use with the Dubins Set.

The conversion [12] from aircraft bearing angles to heading angles and then into a ground coordinate system is necessary so as to obtain the appropriate inputs to the Dubins Set algorithm; and more importantly to be used in the identification of the *IP* and the *WP* quadrants used in this work. Shkel and Lumelsky [10] developed a look-up decision table that simplifies the tedious work of finding all the Dubins permissible trajectories using a starting and ending quadrant approach.

With the optimal trajectory determined the next step is to evaluate the aircraft flight for both the gliding and powered sequences. The performance of aircraft during flight is well documented. Fig. 1 shows an aircraft in flight at a climb angle γ relative to the horizontal axis. The aircraft mean chord line (body axis) and thrust force vector produced by the aircraft power-plant and measured with respect to the flight trajectory are denoted by α and α_T respectively. Assuming the total weight of the aircraft does not change with flight time $(dm/dt = 0)$.The equations of motion yield (4) and (5).

$$m\frac{d}{dt}(V_\infty \cos\alpha_v + W_x) = -L\sin\alpha_v - D\cos\alpha_v - W\sin\gamma + T\cos\alpha_T \quad (4)$$

$$m\left(\frac{V_\infty^2}{r_c} + \frac{dW_x}{dt}\right) = L\cos\alpha_v - D\sin\alpha_v - W\cos\gamma + T\sin\alpha_T \quad (5)$$

The forces acting on an aircraft are resolved along two mutually perpendicular axis; First tangentially to the flight trajectory and then normally to the flight trajectory in the direction of the lift force.

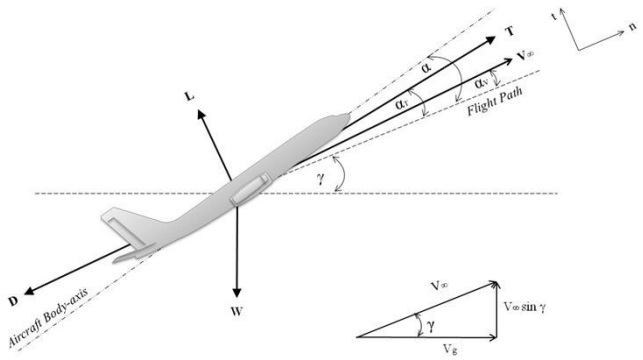

Fig. 1. Aircraft Climbing Flight Trajectory

It is assumed that the flight trajectory direction and relative wind lies along the same line ($\alpha_v \approx 0$), there is no wind during flight ($W_x = 0$), and thrust angle of attack with respect to airspeed vector is very small and approximated as $sin\,\alpha_T \approx 0$ and $cos\,\alpha_T \approx 1$. Therefore (4) and (5) are simplified to:

$$T - W\,sin\,\gamma - D = m\dot{V}_\infty \quad (6)$$

$$L - W\,cos\,\gamma = mV_\infty^2 \quad (7)$$

For steady level flight, the aircraft velocity is constant ($\dot{V}_\infty = 0$) and ($\dot{\theta} = 0$) and the aircraft flight trajectory aligns with the horizontal axis ($\gamma = 0$). Therefore, thrust force is equal to drag force and lift force is equal to the aircraft total weight. The drag and lift forces acting on the aircraft are given by (8) and (9)

$$D = \frac{1}{2}\rho\,V_\infty^2\,S\,C_D \quad (8)$$

$$L = \frac{1}{2}\rho\,V_\infty^2\,S\,C_L \quad (9)$$

It can be shown that the minimum drag airspeed of the aircraft in steady level flight (10) is found from differentiating thrust required to overcome drag in (8) with respect to V_∞ and equating the result to zero.

$$V_{\infty@Dmin} = \sqrt{\frac{2(W/S)}{\rho}\sqrt{\frac{1}{\pi eARC_{D0}}}} \quad (10)$$

where AR (aspect ratio), Oswald efficiency (e) and the zero-drag coefficient (C_{D0}) come from substituting for C_D with the drag polar; $C_D = C_{D0} + ({C_L}^2)/(\pi eAR)$.

The power required is equal to the product of thrust required and aircraft airspeed as shown in (11)

$$P_R = \left[\frac{(1/2)\rho V_\infty^3 C_{D0}}{(W/S)} + \frac{(W/S)}{(1/2)\pi eAR\rho V_\infty}\right]W \quad (11)$$

Similarly, differentiating (11) with respect to V_∞ and equating the result to zero results to the equation of the airspeed for the minimum power required, which is also the minimum sink rate airspeed as shown in (12)

$$V_{\infty@P_{Rmin}} = \sqrt{\frac{2(W/S)}{\rho}\sqrt{\frac{1}{3\pi eARC_{D0}}}} \quad (12)$$

The aircraft maximum flight airspeed is obtained when the maximum power available (P_{Amax}) from the aircraft propeller is equal to the power required at maximum throttle setting and specific altitude ($P_{Amax} = P_R$). Substituting P_{Amax} for P_A and $V_{\infty max}$ for V_∞ into (11) and rearranging accordingly yields (13). The maximum positive root of $V_{\infty max}$ obtained after solving (13) is the maximum airspeed of the aircraft at that specific altitude and throttle setting.

$$\left(\frac{\rho^2 e\pi ARC_{D0}}{4}\right)V_{\infty max}^4 - \left(\frac{\rho\pi e\mathrm{ARP_{Amax}}}{2\mathrm{S}}\right)V_{\infty max} + \frac{\mathrm{W}}{\mathrm{S}} = 0 \quad (13)$$

The optimal climb angle of the UAV glider is achieved at its maximum lift-to-drag ratio conditions. For a steady flight, the optimal climb angle is found from (14)

$$\gamma_{opt} = \frac{T}{W} - \frac{1}{(L/D)_{max}} \quad (14)$$

The optimal climb rate is given by (15)

$$V_{Copt} = V_{\infty@Dmin}\sin\gamma_{\mathrm{opt}} \quad (15)$$

The BUM estimates the percentage energy required of a glider, the flight-time to fly any given trajectory, and the glider final altitude.

B. Altitude Gain Model

Based on *a priori* atmospheric thermal identification, the Altitude Gain Model (AGM) is developed to estimate expected altitude gain from a thermal known strength, size, latitude/longitude location and altitude. Within the thermal, the primary assumption is that the glider airspeed is maintained at minimum sink rate airspeed so as to stay longer in the thermal and achieve higher altitude gain. There are two different techniques employed in thermalling; Circling around the thermal and flying straight across the thermal (exiting and returning). For this work, thermal circling technique is used. The glider exits the thermal at an altitude close to the maximum altitude of the thermal. This technique leads to long thermalling time depending on the thermal's strength, width, and altitude and may penalize a very strong thermal in case the mission is time critical.

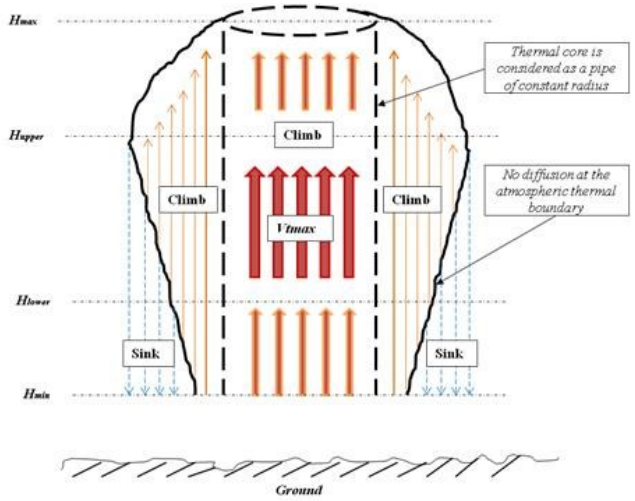

Fig. 2. Updraft Velocity Distribution within the Thermal

Atmospheric thermals observed in practice vary in strength, altitude and the range they cover. Irving [12] observed strong thermals of core strength of up 20 ft/sec and radius of about 787 ft. According to Fonseka [13], thermals reach an upper altitude of up to 3300 ft and a bottom width of 49ft. Previous work by Edwards [6] shows that predicting atmospheric thermal parameters while inside it is indeed an achievable task. The energy gain from the atmospheric thermal is in the form of altitude gain caused by the updraft velocity.

Different mathematical thermal models have been developed to explain the complicated nature of atmospheric thermals. For instance, Fonseka describes the updraft velocity distribution along the thermal altitude using equations (16) through (20). The updraft profile takes a plume form as shown in Fig. 2. In this case the assumptions made are: thermal boundaries are insulated from the outside, horizontal velocity in an atmospheric thermal is negligible in all weather conditions and the global wind influence on the thermal tube is also ignored.

$$\begin{cases} & if\ Z \in [H_{min}, H_{low}] \\ V_t(z) & = \frac{V_{tmin}-V_{tmax}}{(H_{min}-H_{low})^2}Z^2 - 2H_{low}\frac{V_{tmin}-V_{tmax}}{(H_{min}-H_{low})^2}Z \\ & + \quad V_{tmax} - H_{low}^2\frac{V_{tmax}-V_{tmin}}{(H_{min}-H_{low})^2} \end{cases} \quad (16)$$

$$\begin{cases} if\ Z \in [H_{low}, H_{upp}] \\ V_t(z) = \mathrm{V_{tmax}} \end{cases} \quad (17)$$

$$\begin{cases} & if\ Z \in [H_{upp}, H_{max}] \\ V_t(z) & = \frac{V_{tmin}-V_{tmax}}{(H_{max}-H_{upp})^2}Z^2 - 2H_{upp}\frac{V_{tmin}-V_{tmax}}{(H_{max}-H_{upp})^2}Z \\ & + \quad V_{tmax} - H_{upp}^2\frac{V_{tmax}-V_{tmin}}{(H_{max}-H_{upp})^2} \end{cases} \quad (18)$$

where; H_{min} and H_{max} are the altitudes at which the thermal bottom and top are located respectively. H_{low} and H_{upp} define thermal regions of minimum updraft velocity and maximum updraft velocity; they are calculated using (19) and (20) respectively.

$$H_{low} = H_{min} + \frac{1}{5}(H_{max} - H_{min}) \quad (19)$$

$$H_{upp} = H_{min} + \frac{2}{5}(H_{max} - H_{min}) \quad (20)$$

The other two parameters that are necessary to describe the flight trajectory of the UAG are $H_{initial}$ and H_{final} which are the altitude at the beginning of thermal soaring and the altitude of the glider as it exits the thermal. Given minimum updraft strength (V_{tmin}), maximum updraft strength (V_{tmax}), H_{min}, H_{max}, $H_{initial}$, H_{final} and R_t values, the corresponding plot of the updraft velocity, $V_t(z)$, versus change in thermal altitude is shown in Fig. 3.

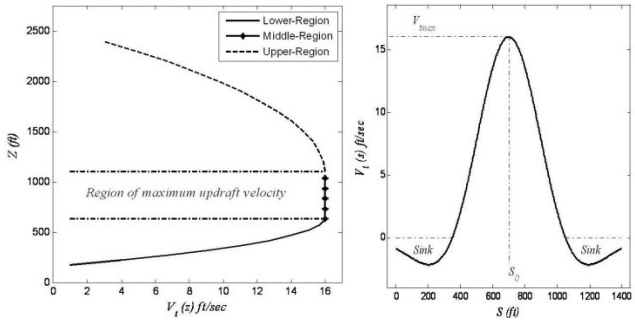

Fig. 3. Updraft velocity distribution along thermal altitude (left) and across thermal range (right)

It is evident that updraft velocity increases rapidly in the lower region, becomes maximum in the middle region and diminishes gradually in the upper region.

A model by Gedeon [14] used to describe flights of dolphin-style thermal soaring and adopted in this research for analysis of updraft velocity distribution along the thermal width / range $V_t(s)$ is given by (21).

$$V_t(S) = V_{tmax}\, e^{-\left(\frac{S-S_0}{R_t}\right)^2}\left(1-\left(\frac{S-S_0}{R_t}\right)^2\right) \quad (21)$$

where S is the specific thermal range and S_0 is the center of the thermal. According to [14] the optimal bank angle of a glider circling around the thermal must satisfy (22),

$$3\,tan^4\,\phi_{opt}\,cos^{\frac{1}{2}}\phi_{opt} = 4\left(\frac{V_{s,min}^2}{gR_t}\right)^2\left(\frac{V_{tmax}}{V_{s,min}}\right) \quad (22)$$

and the optimal climb rate is found according to (23),

$$V_{C_{opt}} = V_{s,min}\left[\frac{V_{tmax}}{V_{s,min}}\left(1-\left(\frac{V_{s,min}^2}{gR_t}\right)^2 cosec^2\phi_{opt}\right) - sec^{\frac{3}{2}}\phi_{opt}\right] \quad (23)$$

The AGM estimates the UAG thermalling-time from $H_{initial}$, H_{final} at an optimum climb rate, $V_{C_{opt}}$.

C. Intelligent Decision Model

Given the results of the BUM and the AGM, the Intelligent Decision Model (IDM) compares the energy benefit and the flight-time for the thermal path (*TP*) with the nominal-path (*NP*). The thermal-path is the trajectory that connects the current location to the next waypoint through a candidate atmospheric thermal location. The nominal-path is the trajectory that connects the current location and the next waypoint directly.

The IDM is developed using a fuzzy logic concept approach. Some recent applications of the fuzzy logic concept relevant to UAVs are evident in Sumita [15]. It focuses on in-flight planning and avoidance of UAVs. Wu et.al. [16] in his work focuses on human-like reasoning and decision-making of UAVs using fuzzy logic approach.

The inputs to the IDM come from the two candidate trajectories under comparison. The output is the level of confidence and recommendation for each trajectory given the desired mission urgency classification. For the current research problem, the two inputs to the IDM are the difference in battery energy levels (ΔE_f) also called Energy Benefit, shown in (24). The other one is the ratio of the *NP* and the *TP* flight-times (t_f) as shown in (25),

$$\Delta E_f = E_{TP} - E_{NP}\ (\%) \quad (24)$$

$$t_f = (t_{NP}/t_{TP})\ \times 100\% \quad (25)$$

where E_{TP} and E_{NP} are the waypoint battery energy levels and t_{TP} and t_{NP} the waypoint flight-times for the *TP* and *NP* respectively.

The flight mission is specified as either *Mission Time-Free* $(t_f \geq 10\%)$ or *Mission Critical* $(t_f \geq 50\%)$ by the user and it is used in setting the membership functions for the fuzzy sets.

It is important to note that there is a normalization step at the conclusion of both prediction paths. In order to make a proper comparison of the Thermal-Path and the Nominal-Path the final altitude from both flight paths must be the same. This is accomplished by one additional iteration of the BUM by the UAG at the lower predicted altitude.

III. Results & Discussion

The UAG used in this example is a scale-size powered glider modeled after a DG-600 sailplane. It is 19.3(lbs) with a HQ 2.5/12 airfoil. Its wingspan and wing area are 209.7(in) and 1764 (in^2) respectively. It uses an 800W brushless motor for propulsion when climbing. The UAG desired altitude range is between 1000ft and gliding to 200ft AGL before climbing again unless a thermal is used to obtain higher altitudes.

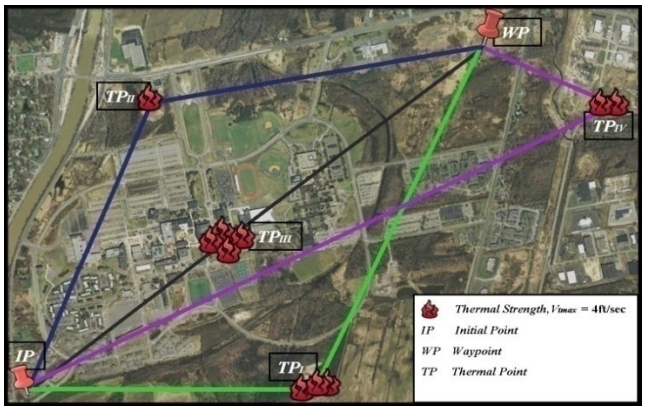

Fig. 4. The UAG Flight Mission Plan

A Flight Mission Plan (*FMP*) comprising of an Initial Point (*IP*) and a Waypoint (*WP*) is set for a UAG flying across the Rochester Institute of Technology campus as shown in Fig. 4. The objective of the mission is to routinely carry out surveillance at the *WP* and fly back to the *IP*. This flight routine is repeated uniformly until the UAG runs out of fuel. In this paper, only a single representative flight routine from *IP* to *WP* directly and through various *TPs* is analyzed. Four different candidate atmospheric thermals

	Long. (deg)	Lat. (deg)	V_{tmax} (ft/sec)	R_t (ft)	H_{bot} (ft)	H_{top} (ft)
IP	-77.68669	43.07893				
WP	-77.65730	43.09088				
TP_I	-77.67047	43.07677	12	200	170	2800
TP_{II}	-77.67665	43.09034	4	200	180	1800
TP_{III}	-77.67161	43.08479	16	480	150	4000
TP_{IV}	-77.68690	43.07954	8	450	210	3000
	ψ_i (deg)	ψ_f (deg)	V_{t_core} (ft/sec)	Bank (deg)	Climb (ft/s)	
TP_I	140	50	7.01	22.2	0.554	
TP_{II}	110	100	2.34	17.2	0.342	
TP_{III}	70	70	9.35	15.7	4.734	
TP_{IV}	80	60	4.67	13.7	1.843	

Table 1. Coordinates, Properties and Bearing angles for *IP*, *WP* and each *TP*

(TP_I, TP_{II}, TP_{III} and TP_{IV}) of different strength, size, and location are identified by a Thermal Identification Algorithm

(*TIA)*. One such embodiment of the *TIA* would be a thermal inferred camera with accompanying image processing capability.

The geographical coordinates for the *IP*, *WP* and each of the *TP* along with the assumed values for the thermal core width, bottom and top altitudes for each thermal are given in Table 1. Also shown are; updraft velocity at the core radius of the thermal, optimal bank angle and optimal climb rate.

From the *IP,* four trajectories are sketched, each linking the *IP* to the *WP* through the *TP*. The first trajectory links *IP* to *WP* through TP_I and is called *IP-*TP_I*-WP* trajectory. Other trajectories are abbreviated in the same fashion. The bearing angle of the *IP* is assumed to be 70° and the desired bearing angle at the *WP* is assumed 250°. The initial bearing angle (ψ_i) and final bearing (ψ_f)angle for each thermal point are given in Table 1. Applying the Dubins set algorithm, the optimal trajectories for each path are determined. The trajectories are then "unwrapped" to allow calculation of the fuel usage along a 1D path. Fuel usage for banked flights inside and outside the *TPs* is outside the scope of this research. Fig. 5 is the Nominal-Path (*IP-WP*) and the Thermal-Path (*IP-*TP_I*-WP*) trajectory plot. Fig.6 is the corresponding unwrapped trajectory. Between the candidate *TPs* and the *WP* and between the candidate *TPs* and the *IP,* the UAG is flying at the minimum drag airspeed which is equal to 35.2 ft/sec (10). The glider flies in the thermal at the minimum sink rate airspeed of 26.8 ft/sec (12).

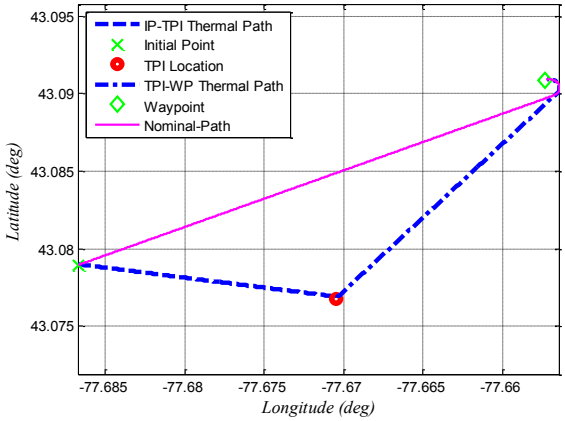

Fig. 5. Dubins Optimal Nominal-Path and TP_I Trajectory

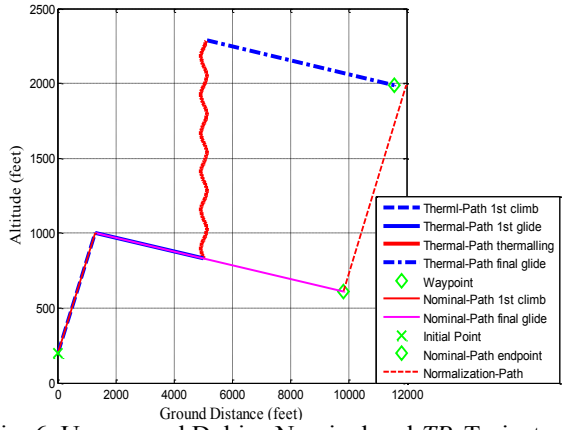

Fig. 6. Unwrapped Dubins Nominal and TP_I Trajectory

Table 2 shows the total flight-time (t_{Tot}) and current battery status $(E_{current})$ at the *WP* for each trajectory. In each case the minimum updraft velocity is assumed 1 ft/sec.

The two parameters under comparison at the *WP* are the total flight-time and the fuel level status as a function of the full fuel capacity. In order for this comparison to be valid, the two trajectories have to be at the same altitude. The NP altitude is normalized to the *TP* aircraft altitude at the *WP*, by performing another climb that starts from NP endpoint altitude and ends at an altitude equal to the current *TP* altitude at the *WP*. Consequently, BUM is re-applied. The power required to perform the Normalization Path and flight-path from *IP* to *WP* are added together, resulting in total power required $(P_{R,NP})$ for the NP at the same altitude as the *TP* at the *WP*. The total flight-time for the NP is also the algebraic sum of the flight-time for flight-path *(IP-WP)* and Normalization-Path. Fig. 6 is an illustration of both the NP and *TP* flight-paths with a normalization step. Note that P_R in Table 2 at the end of the *TP* for each trajectory is the same. This is because fuel is used to climb once for all *TPs*.

Trajectory	$t_{IP\text{-}TP}$ (min)	$t_{Thermal}$ (min)	$t_{TP\text{-}WP}$ (min)	t_{Tot} (min)	$P_{R\ IP\text{-}TP}$ (%)	$E_{current}$ (%)
IP – TP_I - *WP*	2.45	7.517	3.109	13.08	12.4	87.6
IP – TP_{II} - *WP*	2.50	34.18	2.744	39.44	12.4	87.6
IP – TP_{III} - *WP*	2.44	8.250	2.285	12.98	12.4	87.6
IP – TP_{IV} - *WP*	5.42	17.71	23.13	24.28	12.4	87.6

Table 2: Flight-Time and Percentage Power Required for each FPM Trajectory

Trajectory	E_{NP} (%)	E_{TP} (%)	ΔE_f (%)	t_{NP} (min)	t_{TP} (min)	t_f (%)
IP - TP_I -*WP*	66.7	87.6	20.9	6.34	13.1	48.4
IP – TP_{II} -*WP*	77.5	87.6	10.1	5.51	39.4	13.9
IP - TP_{III} -*WP*	51.3	87.6	36.3	7.53	12.9	58.0
IP - TP_{IV} -*WP*	60.0	87.6	27.6	6.86	24.3	28.2

Table 3: Energy-Benefit and Flight-Time Ratio Values for each Trajectory– *Mission Critical*

Inputs to the IDM are: Energy-benefit (24) and flight-time ratio (25). For each *TP* compared to *NP*, the values of ΔE_f and t_f are shown in Table 3. Both IDM inputs; ΔE_f and t_f are divided into five fuzzy sets, Table 4 (for the *Mission Critical* condition). The universe of discourse for input fuzzy sets is defined at [0%, 100%].

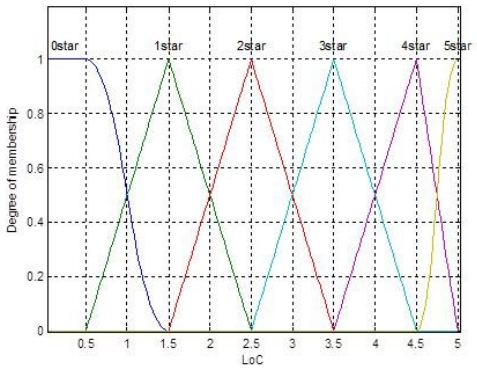

Fig. 7. *LoC* Fuzzy Sets Membership Functions

The output from the IDM is in the form of the Level of Confidence and Recommendations and is divided into six fuzzy sets (0-5 stars), Table 4. Fig. 6 presents membership functions used in determination of *LoC*. Due to the strict mission critical nature desired, only TP_{III} registers a meaningful *LoC* of 2.196, Table 6. It is worthy to note that these confidence ranges are entirely user dependent as illustrated when the mission criticality is relaxed.

Input - t_f	**Range [0 100]**	**Input - ΔE_f**	**Range [0 100]**	**Output – *LoC***	**Range [0 5]**
good	50-70	smaller	0-20	0 star	0- 1.5
very good	60-80	small	0-40	1 star	0.5- 2.5
very, very good	70-90	average	20-60	2 star	1.5- 3.5
excellent	80-100	high	40-80	3 star	2.5- 4.5
perfect	90-100	higher	60-100	4 star	3.5 - 5
				5 star	4.5 - 5

Table 4: Inputs and Output Fuzzy Sets – *Mission Critical*

Input - t_f	**Range [0 100]**	**Input - t_f**	**Range [0 100]**
extremely bad	0-20	good	50-70
very, very bad	10-30	very good	60-80
very bad	20-40	very, very good	70-90
bad	30-50	excellent	80-100
fair	40-60	perfect	90-100

Table 5: Inputs Fuzzy Sets – *Mission Time-Free*

For the *Mission Time-Free* case, the threshold number for flight-time ratio decreases to t_f < 10%. In this case, the number of the input t_f fuzzy sets increases to ten as shown in Table 5. The number of fuzzy sets for the ΔE_f input and *LoC* output remain unchanged as five and six respectively. The total number of fuzzy logic rules increases to 50. These new t_f fuzzy sets for *Mission Time-Free* together with the ΔE_f and *LoC* fuzzy sets are used into the IDM to draft new recommendations as shown in Table 7 based on the flight-time criterion specified. By lowering the flight-time ratio to *Mission Time-Free* all the candidate thermals identified on the FMP can be considered for thermalling.

Trajectory	**Score**	***LoC***	**Recommendation**
$IP - TP_I$ - WP	0	0 star	do not fly the TP
$IP - TP_{II}$ - WP	0	0 star	do not fly the TP
$IP - TP_{III}$ - WP	2.196	1 star	doubt to fly the TP
$IP - TP_{IV}$ - WP	0	0 star	do not fly the TP

Table 6: Level of Confidence and Recommendations for *Mission Critical*

Trajectory	**Score**	***LoC***	**Recommendation**
$IP - TP_I$ - WP	4.115	3 star	good idea to fly the TP
$IP - TP_{II}$ - WP	1.070	1 star	doubt to fly the TP
$IP - TP_{III}$ - WP	4.534	4 star	very good idea to fly the TP
$IP - TP_{IV}$ - WP	3.833	3 star	good idea to fly the TP

Table 7: Level of Confidence and Recommendations for *Mission Time-Free*

IV. CONCLUSION

This research work led to the development of three models to be used on an Unmanned Aerial Glider. The energy cost and flight-time associated with flying the optimal path for both a Nominal and Thermal-paths were calculated using the BUM. The altitude gain from an identified candidate thermal and the thermalling time were obtained using the AGM. Through the IDM the Nominal-path is compared to a Thermal-path using a fuzzy logic approach considering energy efficiency. The decision to fly the thermal-path depends on the mission criticality. For a more thorough treatment of this work see Kagabo [17].

REFERENCES

[1] M. J. Allen and V. Lin, "Guidance and Control of Autonomous Soaring Vehicle Flight Test Results," in *45th AIAA Aerospace Sciences Meeting and Exhibit*, Reno, Nevada, 2007.

[2] M. J. Allen, "Autonomous Soaring for Improved Endurance of a Small Uninhabited Air Vehicle," in *43rd AIAA Aerospace Sciences Meeting and Exhibit*, Reno, Nevada, 2005.

[3] M. J. Allen, "Guidance and Control of Autonomous Soaring UAV," USA Patent 7,431,243 B1, Oct. 7, 2008.

[4] J. W. Langelaan, "Gust Energy Extraction for Mini and MicroUninhabited Aerial Vehicles," *AIAA Journal of Guidance, Control, and Dynamics*, vol. 32, no. 2, pp. 464-473, Mar. 2009.

[5] J. W. Langelaan and G. Bramesfeld, "Gust Energy Extraction for Mini- and Micro-Uninhabited Aerial Vehicles," in *46th AIAA Aerospace Sciences Meeting and Exhibit*, Reno, Nevada, 2008.

[6] D. J. Edwards, "Implementation Details and Flight Test Results of an Autonomous Soaring Controller," in , Honolulu, Hawaii, 2008, p. AIAAGuidance,Navigation and Control Conference and Exhibit.

[7] J. Wharington, *Autonomous Control of Soaring Aircraft by Reinforcement Learning. PhD Thesis*. Melbourne, Austrailia: Royal Melbourne Institute of Technology, 1998.

[8] C. Q. Ying and J. Z. Yiyuan, " Energy-Efficient Trajectories of Unmanned Aerial Vehicles Flying through Thermals," *Journal of Aerospace Engineering*, vol. 18, no. 2, pp. 84-92, Apr. 2005.

[9] L. E. Dubins, "On Curves of Minimal Length with a Constraint on Average Curvature, and with Prescribed Initial and Terminal Positions and Tangents," *American Journal of Mathematics*, vol. 79, no. 3, p. 497–516, Jul. 1957.

[10] A. M. Shkel and V. J. Lumelsky, "Classification of the Dubins Set," *Robotics and Autonomous Systems*, vl.34, no.4, pp.179-202, Mar. 2001

[11] D. J. Grymin and A. L. Crassidis, "Simplified Model Development and Trajectory Determination for a UAV using Dubins Set," in *AIAA Atmospheric Flight Mechanics Conference*, Chicago, Illinois, 2009..

[12] F. Irving, *The Paths of Soaring Flight*. Imperial College Press, 1999.

[13] E. Fonseka, "Modeling and Flying Thermal Tubes with an UAV," ETH Zurich, Zurich, Thesis Report, 2007.

[14] J. Gedeon, "Dynamic Analysis of Dolphin Style Thermal Cross Country Flight," *Technical Soaring*, vol. 3, no. 1, pp. 9-19, 1973.

[15] J. Sumita, "Autonomous NAS Flight Control for UAV by Fuzzy Concept," in *AIAA Guidance, Navigation, and Control Conference and Exhibit*, Providence, Rhode Island, 2004.

[16] P. Wu, P. Narayan, D. Campbell, M. Lees, and R. Walker, "A High Performance Fuzzy Logiv Architecture For UAV Decision Making," in *IASTED International Conference on Computational Intelligence*, San Francisco, CA, 2006, pp. 1-7.

[17] W. B. Kagabo, "Optimal Trajectory Planning For a UAB Glider Using Atmospheric Thermals," M.S. Thesis, Rochester Institute of Technology, Rochester, NY, 2010.